



# Micro-scale spatial variability in soil heat flux (SHF) in a wine-grape vineyard

N. Agam<sup>1</sup> · W. P. Kustas<sup>2</sup> · J. G. Alfieri<sup>2</sup> · F. Gao<sup>2</sup> · L. M. McKee<sup>2</sup> · J. H. Prueger<sup>3</sup> · L. E. Hipps<sup>4</sup>

Received: 1 February 2019 / Accepted: 23 April 2019 / Published online: 7 May 2019  
© Springer-Verlag GmbH Germany, part of Springer Nature 2019

## Abstract

In vineyards, hourly soil heat flux (SHF) may account for as much as 30% of net radiation. Therefore, inaccurate estimates of SHF may lead to non-negligible errors when quantifying the surface energy balance. The typical canopy height to width ratio of two along with widely spaced rows (row spacing exceeding canopy height), and leaf biomass concentrated in the upper half of the vine canopy result in variable shading conditions producing sharp, sometimes abrupt, differences in SHF between adjacent points within the interrow space. Drip irrigation, which is also a typical practice in many vineyards in semi-arid regions, adds an additional source of variability in the interrow soil moisture which strongly affects SHF. Lastly, the common practice in Californian wine-grape vineyards to plant cover crop in the interrow, forming two distinct areas below the canopy—bare soil and crop cover, further increases SHF variability in the interrow. This small-scale variability challenges the measurement of SHF in such agrosystems. The objective of the research was to assess the micro-scale (within the interrow between two vine rows) spatial variability in SHF, and to determine which of the three variables—non-uniform (in both space and time) shading patterns, non-uniform surface cover (bare soil vs. cover crop) and non-uniform soil water content (due to the drip irrigation)—is the most significant driver for the local heterogeneity. The variability of incoming solar radiation reaching the ground was found to be the primary source for the spatial and temporal variation of SHF once the vine canopy was fully developed. The water content distribution and the grass cover in the interrow both had minor impacts on the spatial and temporal variation in SHF. It was further found that a transect of five equally distributed sensors across the interrow accurately represented the area-average SHF given by the 11-sensor array, particularly during the growing season.

## Introduction

In vineyards, hourly soil heat flux (SHF) may account for as much as 30% of net radiation (Heilman et al. 1994). Therefore, inaccurate estimates of SHF may lead to non-negligible

errors when quantifying the surface energy balance (Hsieh et al. 2009). Due to both the natural variability of soils and the micro-environmental variability in sparse canopies, it is a challenge to measure a field-representative SHF, necessitating multiple measurements per site. Although the spatial variability of SHF has been studied before in sparse natural vegetation (Kustas et al. 2000) and in a cotton field (Agam et al. 2012) amongst others, it has not been thoroughly explored in vineyards before.

Wine-grape vineyards typically have a unique architecture with tall canopy (~2 m) that is concentrated at the upper half of the vine height, and widely spaced rows (~3 m). Depending on the row orientation of the vineyard, this architecture results in a mosaic of sunlit and shaded areas at the soil surface that can rapidly change over time. This sunlit-shaded pattern is one of the prime governors of the spatial variation in SHF (Colaizzi et al. 2016).

An additional contributor to the local-scale spatial variability in SHF is the presence of interrow cover crops. Cover crops provide important agro-ecosystem services

---

Communicated by L. Testi.

✉ N. Agam  
agam@bgu.ac.il

<sup>1</sup> Blaustein Institutes for Desert Research, Ben-Gurion University of the Negev, Sede-Boqer Campus, 84990 Midreshet Ben-Gurion, Israel

<sup>2</sup> USDA-ARS, Hydrology and Remote Sensing Laboratory, Beltsville, MD, USA

<sup>3</sup> USDA-ARS, National Laboratory for Agriculture and the Environment, Ames, IA, USA

<sup>4</sup> Plants, Soils and Climate Department, College of Agriculture and Applied Sciences, Utah State University, Logan, UT, USA

such as decrease erosion, improve infiltration and reduce runoff, improve soil tilth, improve soil nutrient retention, help control biomass (vine and berry) production, and build soil organic matter (Battany and Grismer 2000; Hatch et al. 2011; Jackson 2000; Tesic et al. 2007). Ultimately, the presence of cover crop contributes to improving vine microclimate, thus improving wine quality (Morlat and Jacquet 2003). In California, vineyard cover crops are typically planted in the fall at the onset of precipitation (ca. October to November), receive no irrigation, and grow throughout the rainy season into late spring (ca. March to April) while the grapevines are dormant. They are mowed or tilled around budbreak (Steenwerth and Belina 2008). The cover crops are thus typically green and active during the rainy season (fall through early spring) and largely dormant during most of the growing season (late spring and summer). Grass cover, whether green or dry (e.g., stubble), was reported to reduce the magnitude of SHF (Aase and Siddoway 1980; Enz et al. 1988; Payero et al. 2005). Cover crops in wine-grape vineyards typically only occupy ~2/3 of the soil surface, with the other ~1/3 split evenly under the two vine rows, and left bare (Fig. 1).

The commonly applied drip irrigation practice adds an additional complexity to the spatio-temporal variability of SHF in the vineyard, as it forms a non-uniform regime of soil water content across the interrow. Soil water content, in return, is known to affect the SHF, with higher water contents resulting in greater soil thermal conductivity and, thus, greater SHF for a given temperature gradient (Evetts et al. 1994; Idso et al. 1975).

While some research has assessed the variability in SHF under sparse/clumped vegetation conditions (Kustas et al. 2000; Shao et al. 2008), little has been done with respect to row crops (Agam et al. 2012; Kustas and Daughtry 1990). The unique architecture of wine-grape vineyards and the added complexity of crop cover and drip irrigation are all contributing to a micro-scale complexity. The objective of the research was to assess the micro-scale (within the interrow between two vine rows) spatial variability in SHF, and to determine which of these three variables—non-uniform (in both space and time) shading patterns, non-uniform surface cover (bare soil vs. cover crop) and non-uniform soil water content (due to the drip irrigation)—is the most significant driver

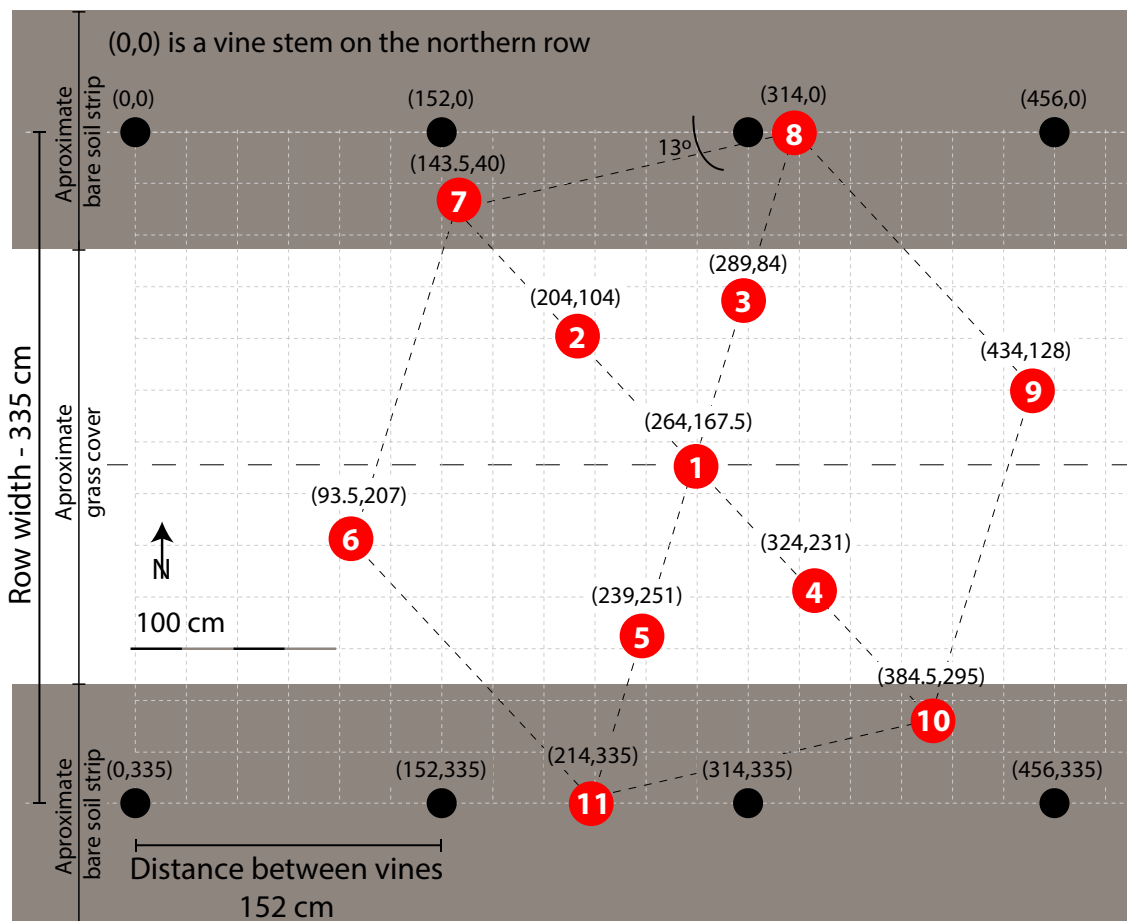


Fig. 1 A schematic design of the soil heat flux array

for this local heterogeneity. Ultimately, the goal was to test if a subset of SHF sensors from a network can provide a reliable average SHF value for the vine and interrow system to be used in energy balance estimation using eddy covariance flux tower measurements.

## Materials and methods

### Site description

The experiment was conducted in a commercial vineyard of Pinot Noir (*Vitis vinifera*) planted in 2009 near Lodi, CA (38.29 N 121.12 W), on a mostly flat terrain as part of the Grape Remote Sensing Atmospheric Profile and Evapotranspiration eXperiment (GRAPEX). The ultimate goal of this ongoing project is to provide wine-grape producers with the tools needed to generate high-resolution evapotranspiration data that can be used to guide water management decisions. More details on the project and the measurements conducted are summarized in Kustas et al. (2018b) as well as in all the papers in this issue.

The local soil is a loam/clay loam. The vine trellises are 3.35 m apart and run in an east–west direction. An individual vine is planted every 1.5 m, with the canopy trained in a bilateral cordon (split canopy) architecture with the two main cordons attached to the first wire at a height of 1.45 m above ground level (agl). Typically, the vines reach a maximum height of 2.0–2.5 m agl during the early part of the growing season with the vine biomass concentrated in the upper half of the total canopy height. The typical vine canopy width is nominally 1 m mid-season. Pruning of the vines is mainly performed to remove shoots growing significantly into the interrow and depending on the weather conditions, often the vines are used to shade the south facing grapes to prevent overexposure of radiation.

The vineyard is drip-irrigated with a dripline positioned directly beneath the center of the vines at a height of ~0.5 m agl. In 2016, irrigation was initiated in mid-April, at the end of the rainy season, during which there was 245 mm of rainfall, of which about 100 mm fell in March–April 2016. The center ~2 m of the 3.35-m interrow between the vine lines is covered with a mixed grass (30% prairie brome; 24% annual ryegrass; 20% tower fescue; 19% blando brome; 7% other) that is allowed to grow in the early stages of the growing season, and then mowed several times in spring and left to cure over the summer. By and large, the grass is dormant throughout most of the growing season, thus barely transpiring

water, and its presence served mostly as an insulation layer.

### Soil heat flux measurements

Soil heat flux was measured using the combination method (Fuchs and Tanner 1968; Hanks and Tanner 1972) according to which a heat flux plate (HFT-3, Radiation Energy Balance Systems, Bellevue, Washington) was deployed at 8 cm depth measuring the soil heat flux at 8 cm ( $G_{\text{SHF}}$ ) to which the heat storage above the plate ( $\Delta G_s$ ) was as added (Eqs. 1a, 1b):

$$G = G_{\text{SHF}} + \Delta G_s, \quad (1a)$$

$$\Delta G_s = \sum_{\text{layer}=1}^2 C_v \frac{\Delta T}{\Delta t} \Delta z, \quad (1b)$$

where the 8-cm layer was split into two layers, 0–4 and 4–8 cm;  $\Delta T/\Delta t$  [ $^{\circ}\text{C s}^{-1}$ ] is the layer-averaged time rate of change in soil temperature;  $\Delta z$  is the thickness of each layer (=0.04 m); and  $C_v$  [ $\text{J m}^{-3} \text{K}^{-1}$ ] is the layer-averaged volumetric heat capacity computed as (Brutsaert 1982)

$$C_v = (1.94 \times \theta_m + 2.5 \times \theta_o + 4.19 \times \theta_w) \times 10^6, \quad (2)$$

with  $\theta_m$ ,  $\theta_o$ , and  $\theta_w$  being the volume fractions of mineral soil, organic matter, water content, respectively. Soil temperatures were measured at the middle depth of each layer, i.e., at 2 and 6 cm using self-made type-E Chromel–constantan thermocouples; and volumetric soil water content was measured with HydraProbes (Stevens Water Monitoring System, Portland, Oregon) installed at a depth of 5 cm, representing the average water content of both layers. Volumetric mineral content fraction was determined based on bulk density measurements conducted in five locations, evenly distributed along a transect between two rows (two repetitions each) using a bulk density sampling tool. Some differences between locations were apparent (Table 1), with location four having the highest mineral content ( $\theta_m = 0.57$ ),

**Table 1** Volumetric mineral content across the interrow

	Location 1	Location 2	Location 2	Location 2	Location 2
Distance from vine row (cm)	0	84	168	251	335
Volumetric mineral content (–)	0.53	0.51	0.48	0.57	0.47

likely due to compaction from tractor wheels, and location five having the lowest ( $\theta_m = 0.47$ ). While these differences are substantial, their effect on total soil heat flux is rather small. A sensitivity analysis conducted to quantify this effect reveals that the range of  $\theta_m$  0.47–0.57 results in a 5% difference in soil heat flux, which corresponds, at maximum, to  $10 \text{ W m}^{-2}$ . The sensitivity of soil heat flux to changes in organic matter content is even smaller, with  $\theta_o$  ranging from 0.01 to 0.05 resulting in less than 4% difference in soil heat flux, which corresponds, at maximum, to  $8 \text{ W m}^{-2}$ .  $\theta_o$  was set to 0.03 based on what is typical organic content observed in US Western soils (personal communication Dr. Scott Jones, Utah State University).

Eleven sets of soil heat flux measurements were deployed in an array between two vine rows as illustrated in Fig. 1. The SHF array was tilted  $13^\circ$  off-north to increase the representation of positions across the interrow (e.g., instead of positions 7 and 8 both representing the position underneath the vine, position 7 is 40 cm south of position 8; and instead for positions 1, 6, and 9 all being in the middle of the interrow, only position 1 is in the middle, while positions 6 and 9 are 40 cm south and north of 1, respectively). Positions 1, 3, 5, 8 and 11 create a linear transect evenly spread across the interrow, corresponding to the SHF measurement protocol used for the GRAPEX flux towers.

All sensors were connected to a datalogger (CR1000 Campbell Scientific Inc., Logan Utah), extended with a multiplexer (AM25T Campbell Scientific Inc. Logan, Utah). The thermocouples and soil heat flux plates were sampled every 30 s and the hydraprobes every 15 min. All were averaged every 30 min. Unfortunately, bulk density measurements were not conducted at each of the 11 points of the array, due to technical limitations. The mean bulk density of all measurements (five locations, two measurements it each;  $\theta_m = 0.514$ ) was used to calculate the fluxes for all locations.

### Below-canopy radiation

Radiation measurements in the interrow below the vine canopy were collected during three intensive observation periods: May 1–2, June 10–11, and July 28–29, 2016. During these periods, radiation divergence was measured by five pyranometers: Kipp and Zonen (CMP11 and CMP21, Kipp & Zonen B.V., Delft, The Netherlands) in the first two campaigns, and Apogee (CS300, Apogee Instruments Inc., Logan, Utah, USA) in the third. The pyranometers were set on a leveling board that was laid across the interrow, so that five positions across the interrow were represented: 30 cm north of the southern row, in the middle of the interrow, 30 cm south of the northern row, and two pyranometers

halfway between the two at the edges and the one in the interrow (30, 90, 150, 210, and 270 cm from the southern row). Additional details and a visual description of the setup can be found in Kustas et al. (2018a; this issue).

### Leaf area index

To define the synoptic changes in vine biomass over the growing season, daily estimates of the leaf area index (LAI) were generated from Landsat and MODIS satellite imagery using the data fusion technique of Gao et al. (2006, 2012, 2014). The resulting 30-m resolution LAI map was then smoothed and gap-filled to generate daily LAI using the Savitzky–Golay filter approach. The details of this procedure and the satisfactory agreement with ground-based LAI observations for this vineyard can be found in Sun et al. (2017). The 30-m LAI pixel over the SHF array was used in this analysis. In a separate study, good agreement was found between the 30-m resolution satellite-derived LAI and ground measurements in the vicinity of the soil heat flux array (White et al. 2019; this issue).

### Monthly average clear-sky days

To account for seasonal changes throughout the growing season, four consecutive days during which clear-sky conditions prevailed were chosen to represent each month from March to October (Table 2). The 4 days were averaged to form a representative mean day for each month.

**Table 2** Clear-sky days used for creating the monthly mean days

Clear-sky days (2016)	LAI (–)	Irrigation (mm)
March		
15–18	1.0	0
April		
15–18	1.6	4.2
May		
15–18	2.1	2
June		
21–24	2.2	19
July		
18–21	2.0	16
August		
16–19	1.7	11.6
September		
14–17	1.7	9.3
October		
18–21	1.5	0

In addition, the mean soil heat flux from all 11 positions and the mean for the 5 transect positions (#1, 3, 5, 8, 11) were computed for each time point ( $SHF_{ARRAY}$  and  $SHF_{TRANS}$ , respectively) for each monthly 4-day average.

### Statistical analyses

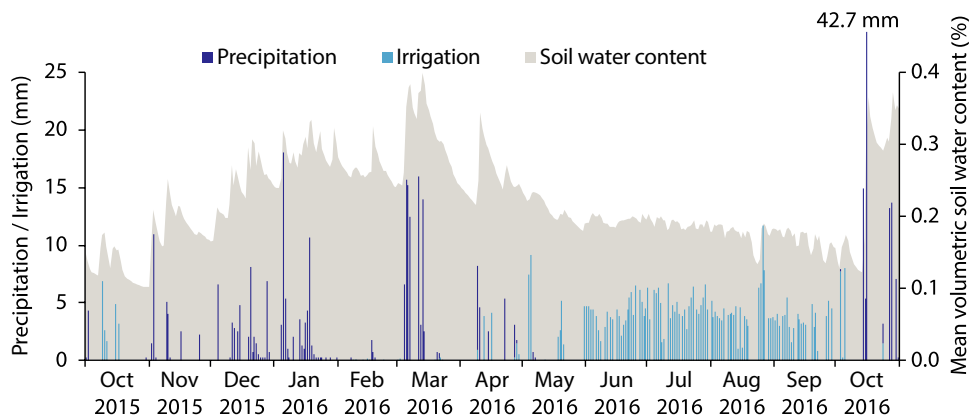
For illustrative purposes, interpolation of soil water content and daily sum of soil heat flux were performed on the 11 measurement positions for the average days in March and July. The interpolation was done using the inverse distance-weighted (IDW) technique which does not make explicit assumptions about the statistical properties of the input data (Watson and Philip 1985). A leave-one-out cross-validation (LOOCV) was performed to assess the quality of the interpolation. The IDW interpolation and its cross-validation were conducted with “gstat” package in R. The LOOCV root mean square values for water content and soil heat flux for the months March and July are presented in Table 3.

To assess the heterogeneity of soil heat flux in the array throughout the season, the monthly four clear-sky average days were used. For each month, the diurnal soil heat flux measurements at the 11 locations were correlated to one another (55 combinations), and the average correlation was computed. Higher mean correlation indicated a more homogeneous distribution of soil heat flux.

**Table 3** Root mean square results from the leave-one-out cross-validation performed for the interpolation of water content and soil heat flux for March and July average days, 2016

	March	July
Volumetric water content (%)	0.033	0.116
Total daily soil heat flux ( $MJ\ m^{-2}$ )	0.697	2.139

**Fig. 2** Precipitation and irrigation (mm) in the vineyard from October 2015 to October 2016. Corresponding mean volumetric soil water content (%) in gray (colour figure online)



## Results and discussion

### Seasonal field conditions: precipitation and irrigation

During the winter preceding the 2016 growing season, precipitation amounted to 247 mm, distributed from October 2015 through April 2016, most of which occurred from November 2015 to January 2016, with 87 mm in March and 23 mm in April. The next rainfall event occurred mid-October 2016. During the dry period between April and October, irrigation supplemented the water balance applying a total of 470 mm. The soil water content (an average across the interrow) corresponding to these water inputs varied during the rainy season, and remained relatively stable (at  $\sim 0.18\%$  volumetric water content) throughout the dry (irrigated) period (Fig. 2). The two water input regimes—precipitation and irrigation—resulted in two distinct spatial distributions of soil water in the vineyard (Fig. 3). When soil water content was dictated by precipitation (Fig. 3a; March), the soil water content was almost uniform across the sampled domain, while under the drip irrigation regime (exemplified for July; Fig. 3b), a clear water content pattern was observed, with higher water content along the driplines underneath the vines (volumetric water content (VWC) of  $\sim 0.25$ ) and a dry interrow (VWC of  $\sim 0.1$ ). The amount of irrigation during the monthly 4-day periods is listed in Table 2.

### LAI dynamics

The total LAI, a combined LAI of the grass and the vine canopy, is presented in Fig. 4. A qualitative illustration of the partitioning between the grass and the vine canopy LAI throughout the season is provided in Fig. 5. The sharp increase in total LAI and the transition from a dominance of the grass to a dominance of the vine canopy from March to May was pronounced. A gradual decrease in LAI from end of May until the end of the season was observed, likely due



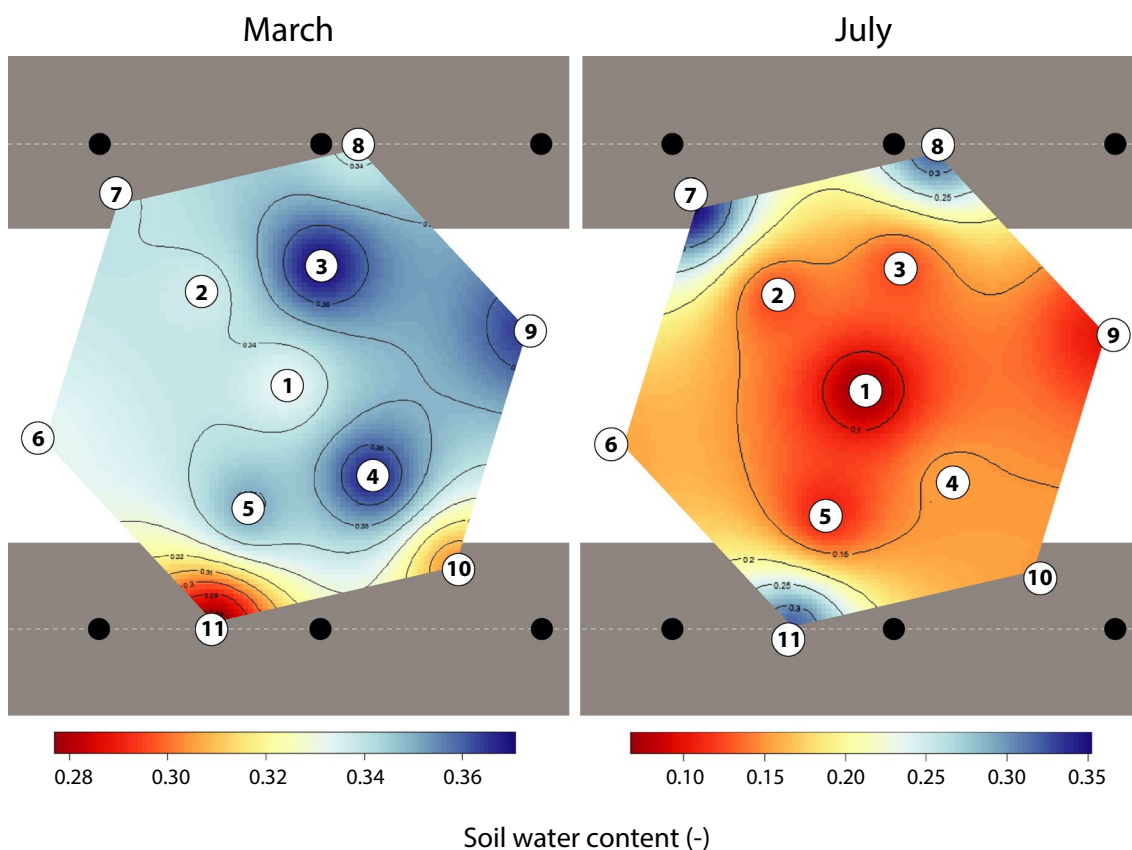
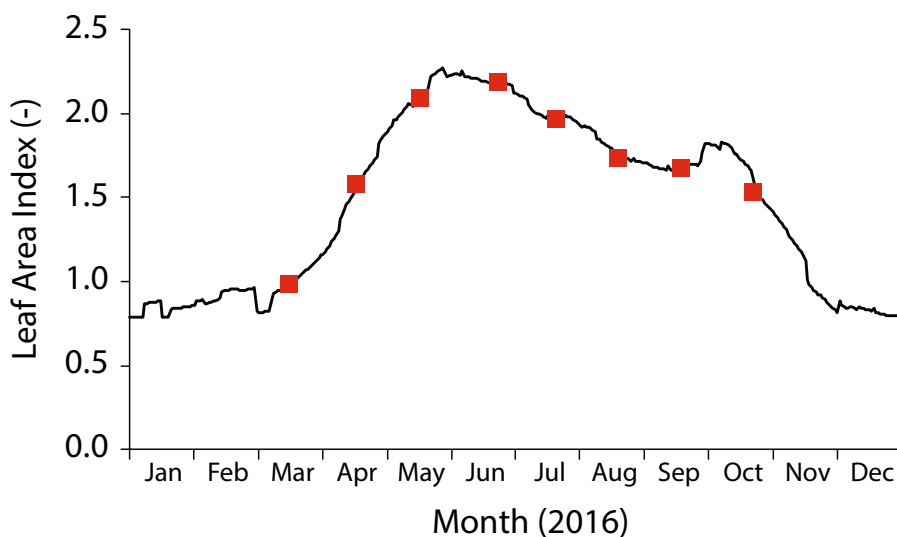


**Fig. 3** Interpolation of the soil water content across the measurement array in March (left) and July (right) 2016. Note the different scale range for the 2 months

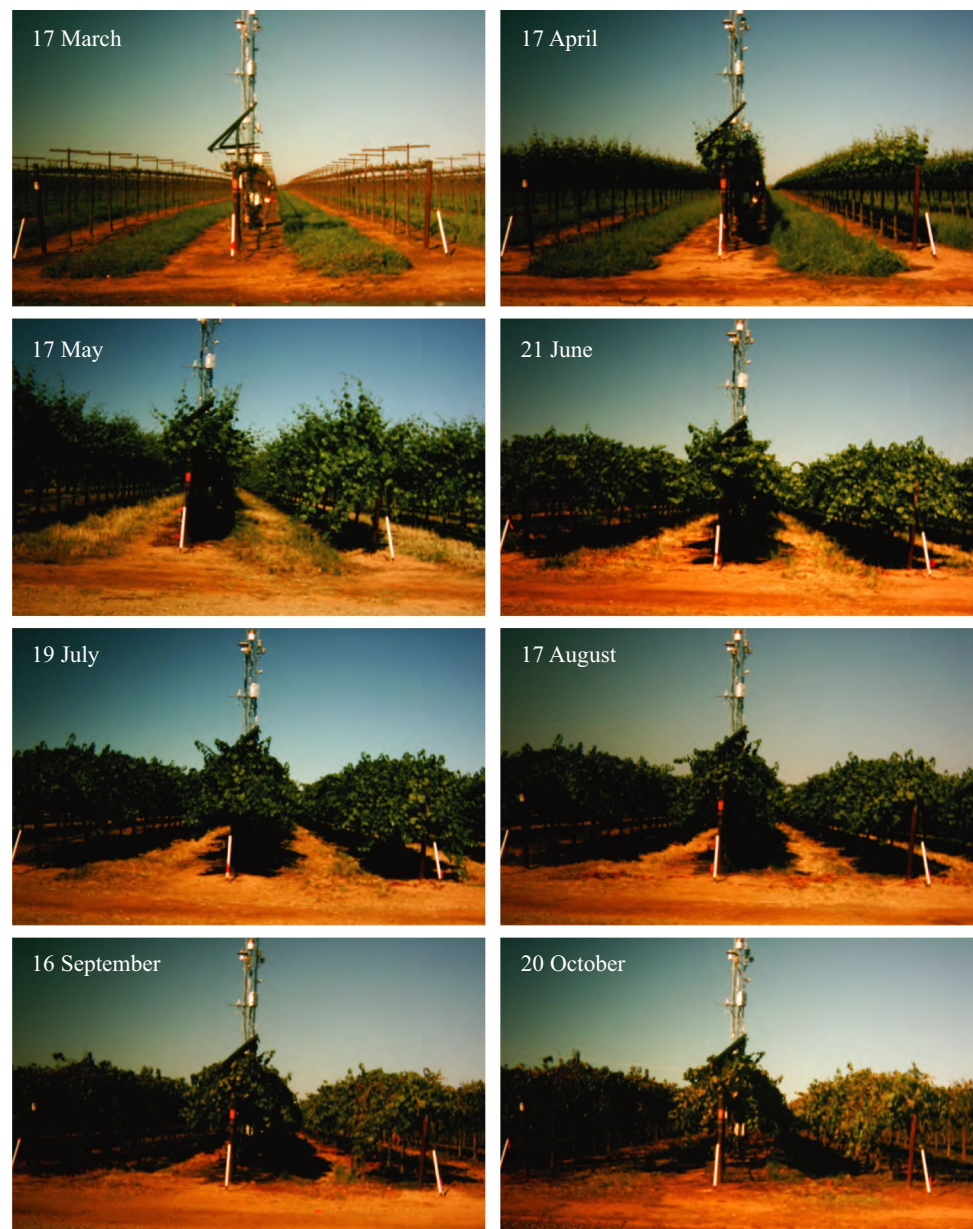
**Fig. 4** Seasonal dynamics of leaf area index. The red rectangles locate the monthly 4-day averages (see Table 2) (colour figure online)



to change in structure over the growing season that change the NDVI signal and fractional cover both contributing to a reduction in apparent LAI. A sharp decrease is observed between October and December. From the end of May through September, the grass was by and large dormant, and

the LAI mostly reflected the vine canopy LAI. Specifically, the LAI in March reflects the grass LAI only, and the LAI in June–September reflects the vine LAI almost exclusively. Exceptions were observed in places where the drip irrigation over-flooded the interrow resulting in local reemergence of

**Fig. 5** Side photographs of the vineyard at one of the four analyzed days each month



the grass. This occurrence was more pronounced in October, when more green grass could be observed. Mean total LAI during the days representing each month is listed in Table 2 and is marked by red squares in Fig. 4.

### **Distribution of below-canopy radiation across the interrow**

The unique architecture of wine-grape vineyards creates a complex below-canopy radiation that rapidly changes at both diurnal and seasonal timescales. A full description of the radiation divergence and its effect on the energy

fluxes below the canopy can be found in a separate paper in this issue (Kustas et al. 2018a). The below-canopy radiation measurements along the transect during the three intensive observation periods are presented in Fig. 6a–c. The large difference in the diurnal pattern of radiation in each of the locations is apparent, and more so, the abrupt change between fully shaded and fully sunlit and the corresponding changes in radiation intensity at each given location are observed. To illustrate the response of soil heat flux to these abrupt changes, the diurnal course of soil heat flux for the five locations in the array that correspond to the pyranometer locations (locations 10, 4, 1, 2,

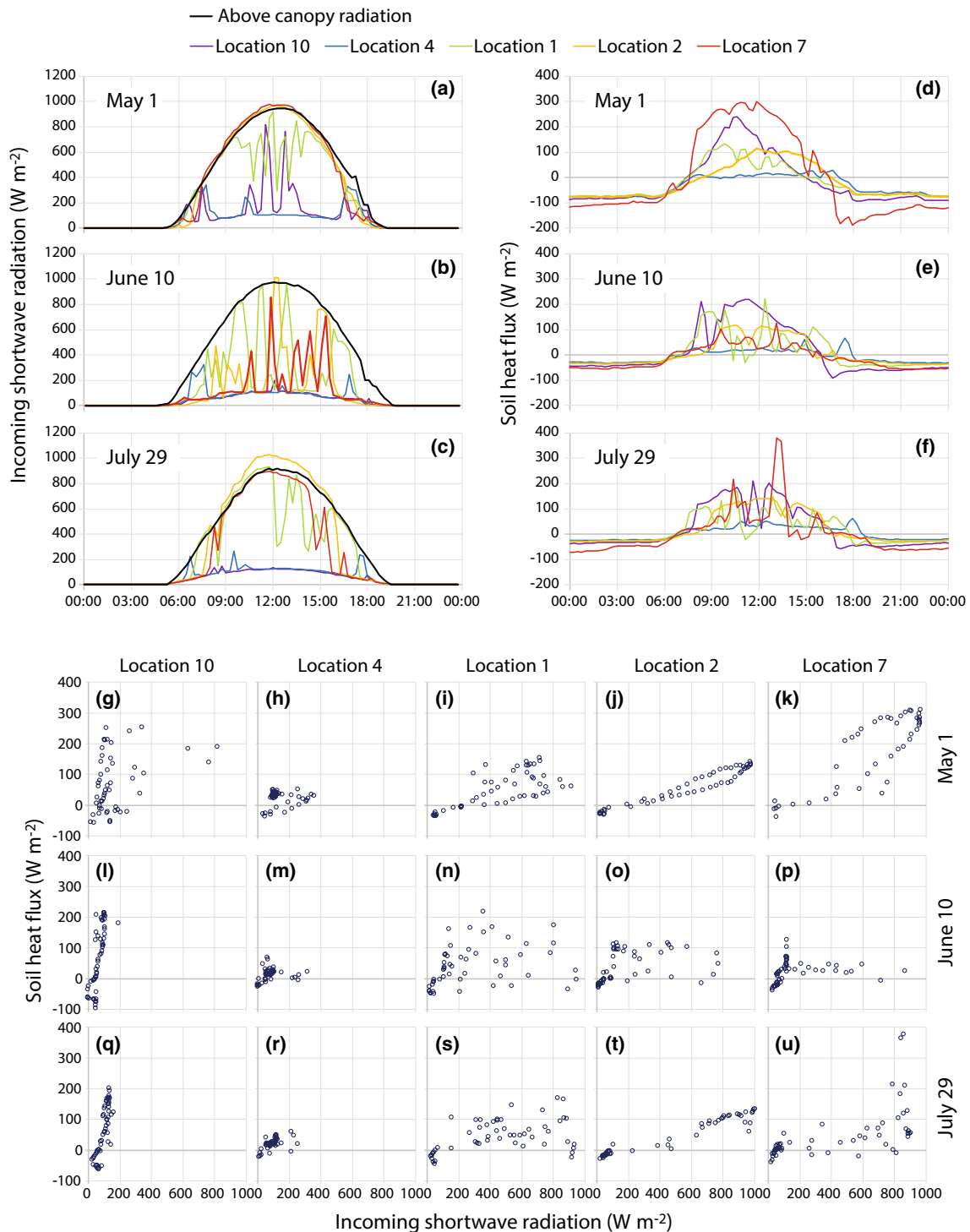


**Fig. 6** Below canopy radiation measurements along the transect during the three intensive observation periods (a–c), and the corresponding diurnal course of soil heat flux (for the five locations where the

pyranometers were set—locations 10, 4, 1, 2, and 7) (d–f). The scatterplots between soil heat flux and below-canopy radiation in each location during the 3 days are in g–u

and 7; Fig. 1) were plotted as well (Fig. 6d, e). If it seems difficult to follow specific patterns it is indeed because such corresponding patterns do not clearly exist. The (lack

of) correlations between the below-canopy radiation and soil heat flux for each location are shown by the scatterplots in Fig. 6g–u.



## Spatial distribution of soil heat flux

In an attempt to separate the effect of the three variables, i.e., shading (or radiative forcing), soil water distribution, and the cover/no cover of grass, the months March and July were chosen. In March, the water content is dictated by rainfall, and is thus more uniform, and being shortly after bud break, the vine canopy has a minimal effect. Thus, variability in soil heat flux is hypothesized to be mostly affected by the intercrop pattern. Due to the rainfall/irrigation conditions in vineyards in this climate, the growth of the canopy coincides with the period when irrigation is the only water source, thus separation between them is not possible. In July, the vine canopy is fully developed, and irrigation is the only water source in the vineyard, while the grass is dormant, representing the conditions persisting during much of the growing season. The spatial variability of SHF in these two distinct conditions is exemplified in Figs. 7, 8 and 9. Figures 7 and 8 present the diurnal pattern of SHF in each of the 11 positions where measurements were conducted (see Fig. 1) using

the 4-day average for March and July, respectively. Figure 9 presents the mean SHF ( $\pm$  standard deviation; STD) composed of all 11 positions for March and July (panels a and b, respectively), and the interpolated spatial distribution of daily sum of SHF in March and July (panels c and d, respectively). While in March there seems to be a small decrease in SHF around noon in the southern  $\sim 1/3$  of the interrow, likely due to short-term shading from the vines infrastructures (see upper left panel in Fig. 5), the magnitude of the fluxes and the overall patterns are more similar compared to the variability in July. In July, the diurnal patterns are not as clear. Positions 8 and 11, the two positions immediately underneath the vines, do follow a “typical” diurnal pattern, but with a very small magnitude ( $\sim \pm 50 \text{ W m}^{-2}$ ; Fig. 8), and even more interestingly, with a negative daily sum ( $< -1.3 \text{ MJ day}^{-1}$ ; see the blueish hues in Fig. 9d), implying that overall, these positions lose more energy than they gain, which is counterintuitive in the Californian summer. The SHFs in positions 2, 3, and 9, located in the northern portion of the interrow but not underneath the northern vine

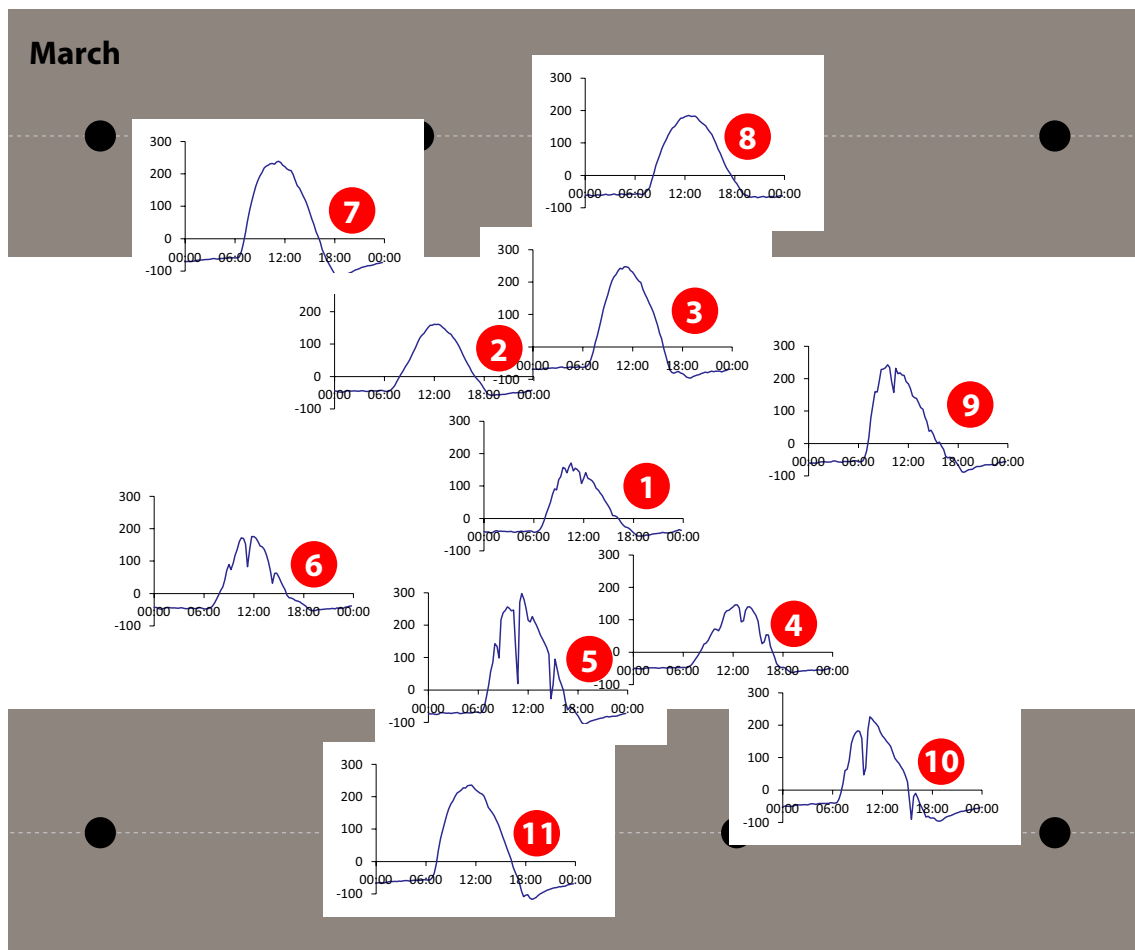


**Fig. 7** Example of the spatial distribution of soil heat flux across the interrow in March 2016. The figures are spread according to the position they represent. The  $x$ -axis is time of day, and the  $y$ -axis is soil heat flux ( $\text{W m}^{-2}$ )

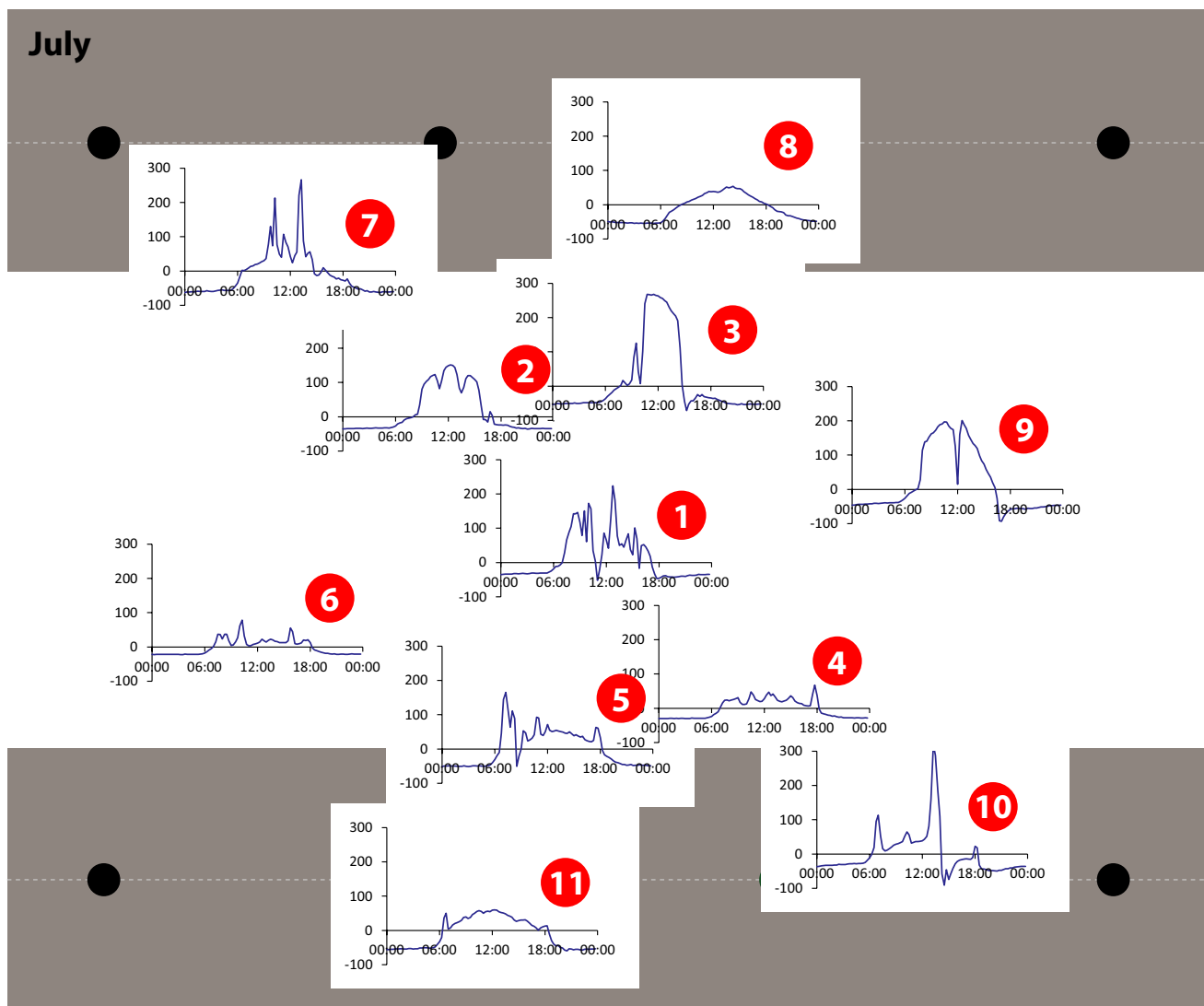


**Fig. 8** Example of the spatial distribution of soil heat flux across the interrow in July 2016. The figures are spread according to the position they represent. The  $x$ -axis is time of day, and the  $y$ -axis is soil heat flux ( $\text{W m}^{-2}$ )

row, show a greater maximum ( $\sim 200 \text{ W m}^{-2}$ ) and a similar minimum ( $\sim -50 \text{ W m}^{-2}$ ) compared to positions 8 and 11 (Fig. 8), resulting in a positive daily sum  $> 2.4 \text{ MJ day}^{-1}$  (the reddish hues in Fig. 9d).

While in March all locations had a positive daily sum of SHF, and except for location 4 showed little variability, as the canopy developed the daily sum of more locations switched from positive to negative (Fig. 10), and that there is a directionality to this behavior. A change in sign started first in the southern locations, i.e., the ones facing north which are the more shaded locations. The daily sum SHF in locations 7 and 8, which are the northernmost also became negative, because they are directly under the vine and are shaded for extended time throughout the day as well. Note that in October, the daily sum of SHF was negative throughout the domain, as the fall season approached with reduced

radiation and cooler temperatures, leading to greater shading of the interrow.

From these analyses of the SHF observations, it is concluded that the daytime SHF is greater in March than in July and that the daytime spatial variability (reflected by the greater STD) is greater in July albeit with a smaller overall flux. In addition, the daily sum of SHF is greater, and positive, in March, throughout the entire domain, while in July it is more variable, and not consistent in sign. This indicates that the proximity between SHF measurements does not guarantee similarity in the magnitude or temporal behavior in SHF rather the position along the interrow is mainly dictating the magnitude and temporal behavior of the flux.

Several factors may be responsible for these results: the differences in the water content regime; the presence of active vs. dormant grass in the interrow; and the incoming

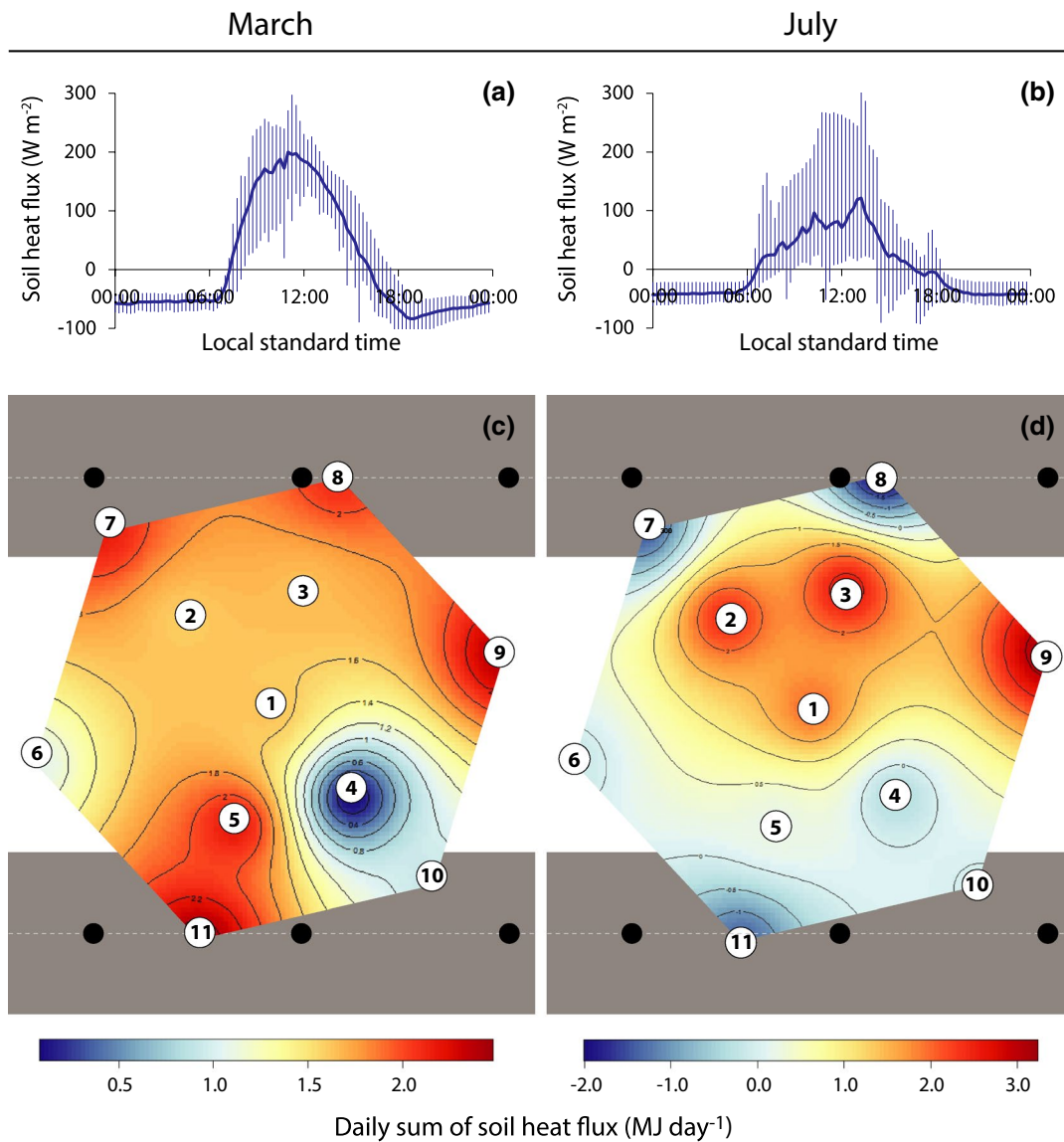


**Fig. 9** The average  $\pm$  standard deviation of soil heat flux from all positions in March (a) and July (b) 2016, and the corresponding interpolation of the daily sum of soil heat flux in March and July (c, d, respectively)

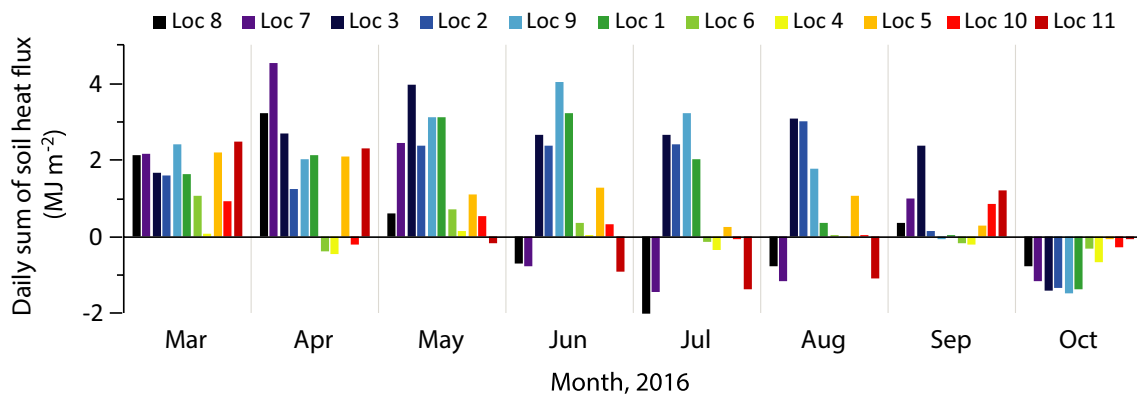


**Fig. 10** Seasonal dynamics of daily sum of soil heat flux at the 11 locations. The location numbers (Loc) are ordered from north to south (see Fig. 1)

shortwave radiation penetrating through the vine canopy (when present).

The soil water content was indeed higher and more uniform in March than in July, which could provide partial explanation for the observed differences in SHF. However, if water content played the only role, one could expect more similarity between the diurnal SHF of positions 1, 6, and 9 (Fig. 8), all located far from the driplines with  $VWC < 0.15$  ( $\text{m}^3 \text{m}^{-3}$ ) (see Fig. 3). In fact, they show very large differences, with position 6 being similar to positions 4 and 5 and position 9 more similar to positions 2 and 3, regardless of soil water content.

The presence of the grass was hypothesized to reduce the SHF as it acts as a buffer layer, shading the soil from direct solar radiation, as well as absorbing some of the heat, and when active, also reducing SHF due to increased latent heat flux. Thus, it was hypothesized that especially in March, when all other conditions are more homogeneous, the SHF under the grassed portion of the interrow will have a smaller diurnal magnitude. To test this hypothesis, the average ( $\pm$ STD) SHF of the grassed positions (1–6, 9) and the bare soil positions (7, 8, 10, 11) for March and July were computed (Fig. 11), and a paired Student's  $t$  test was performed. The  $t$  statistics for March and July were  $-1.24$  and  $6.61$ , respectively, indicating no significant difference between the grass and the bare soil mean SHF in March (two-tailed  $p = 0.22$ ), but a significant difference in July (two-tailed  $p \ll 0.01$ ). In March, the grass insignificantly decreased the SHF. In July, however, while the difference between the grass and the bare soil was statistically significant, the direction of the difference indicates a larger flux under the grass compared to the flux from the bare soil, which cannot be explained by the presence of the grass.

The distribution of shortwave radiation below the vines canopy is discussed in Kustas et al. (2018a; this issue), see particularly the measurements illustrated in their Fig. 4.

Significant variability in below-canopy radiation was observed, reflecting the heterogeneous nature of the spatial and temporal variation in the sunlit and shaded areas below the vine canopy. This was explained by the fact that the vines were not significantly trained and/or pruned for these vineyards and hence the vines growing into the interrow created large variability in shading/canopy cover. Being the source of energy, dissipating into the energy balance components, the variability of incoming solar radiation is concluded to be the primary source for the heterogeneity in SHF distribution in July. In March, the vines only started to leaf out, and created very minimal shading, thus a more uniform distribution of SHF was observed. The seasonal change in SHF heterogeneity, as reflected by the mean of all correlations between pairs of two positions (Fig. 12), proves the strong correlation between SHF heterogeneity and LAI ( $r^2 = 0.89$ ). The water content distribution and the grass cover in the interrow seem to play only a secondary and insignificant role in the SHF distribution.

### Implications on soil heat flux measurements in vineyards

Based on the conclusion that SHF variability is primarily dictated by below-canopy incoming solar radiation, with secondary effects of the grass presence and the water content, it was hypothesized that a mean SHF of the vine row and interrow system could be obtained with a single transect across the interrow. This hypothesis is based on the understanding that the below canopy space can be divided into longitudinal strips: the bare vs. grassed, the wet vs. dry, and the shaded vs. sunlit are all having forms of fuzzy strips. We hypothesized that five sensors along a transect will be able to represent this type of variability. To test this hypothesis, the average SHF from the 11-sensor array was compared to the average SHF derived from positions 1, 3, 5, 8, and 11 that

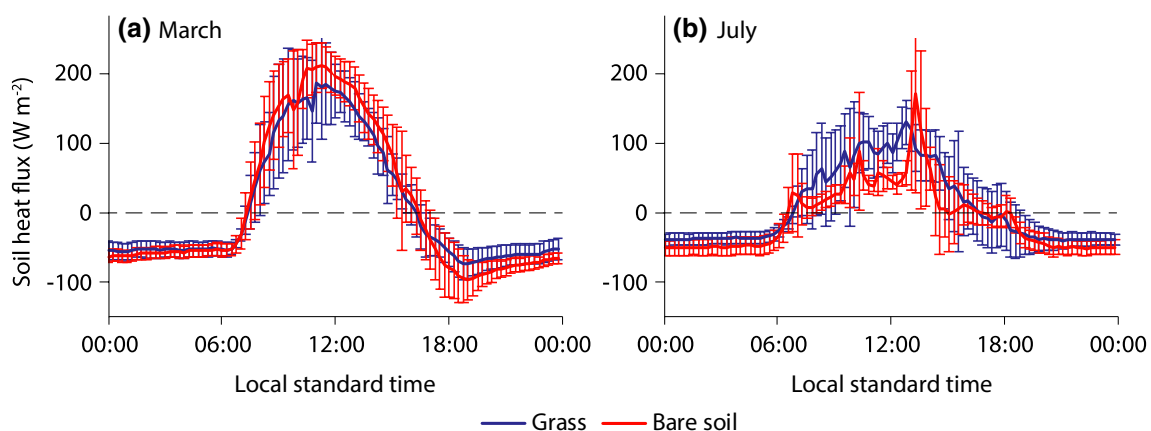
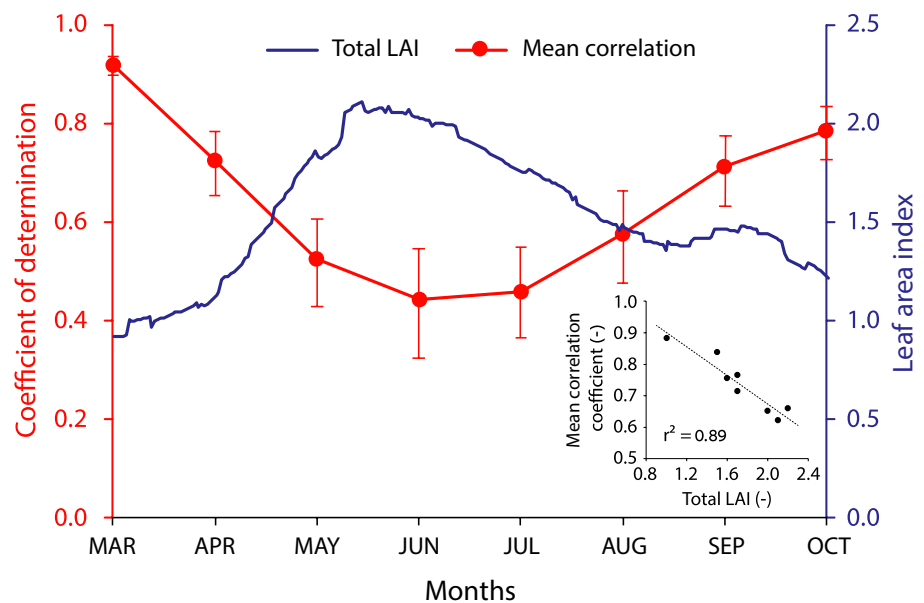


**Fig. 11** The diurnal course of soil heat flux over the grass and the bare soil in March and July 2016

**Fig. 12** Average coefficient of determination between all pairs of positions  $\pm$  standard deviation derived for the monthly 4-day averages, laid over the seasonal leaf area index (LAI). The insert is a scatterplot between LAI and the coefficient of determination



forms a linear, equally distant, transect across the interrow (Fig. 13). There was a generally good agreement between the array and the transect averages ( $SHF_{ARRAY}$  and  $SHF_{TRANS}$ , respectively), especially between May and August. During these months, which are the months with highest LAI, the slope of the least squares regression between  $SHF_{TRANS}$  and  $SHF_{ARRAY}$  ranged from 0.96 to 1.08, and the mean absolute error (MAE) was between 7 and 9  $W m^{-2}$ . These errors are clearly within the measurement uncertainty in SHF, and are thus negligible. In the beginning (March–April) and end (September–October) of the growing season, the transect averages seem to somewhat overestimate SHF compared to the array, but even then, the largest MAE was found to be approximately 15  $W m^{-2}$ , which is still within an acceptable error level for practical purposes. It was thus concluded that an average based on five positions equally distributed along a transect across the interrow accurately represents the field SHF.

Given that in many studies the number of SHF measurement repetitions is three, we further examined the error magnitude one is prone to when instead of the recommended five strategically placed measurements, only three are used. All ten combinations of three out of five were averaged and compared to the five-sensor transect average (Fig. 14). The maximum percent difference between the various three-sensor options and the five-sensor transect average was calculated by dividing, at each time point, the range of SHF calculated from the ten combinations by the five-sensor transect average. Nighttime (21:00–03:00 PST) and daytime (10:00–14:00 PST) were calculated (Table 4). The transition times (from positive to negative SHF and vice versa) were excluded to avoid division by small numbers. None of the ten combinations of the three-sensor placement

accurately follow the five-sensor transect diurnal course, with some producing errors of nearly 100%. Even during nighttime, the errors are in the order of 20% indicating a persistence of daytime surface heating from radiation affecting SHF over night. A clear seasonal effect is apparent in the daytime errors, increasing from March to June, remaining maximal between June and August, and slightly decreasing from August to October, resembling the leaf area seasonal dynamics. These results further support our hypothesis that the three-sensor transect design is better able to capture the effects of radiation water content and cover crop on the average interrow SHF.

## Summary and conclusions

Analysis of the spatial and temporal patterns of SHF measured using an array of 11-sensor sets revealed that the daytime SHF was greater in March than in July, and the daytime spatial variability (reflected by the greater STD) was greater in July albeit having an average smaller flux. The daily sum of SHF was greater and positive in March, throughout the entire domain. It was more variable, and not consistent in sign in July.

The variability of incoming solar radiation was found to be the primary source for the heterogeneous SHF distribution in July, while in March a more uniform distribution of SHF was observed. This resulted in a strong correlation between SHF heterogeneity and LAI ( $r^2 = 0.89$ ). The water content distribution and the grass cover in the interrow seem to have played only a secondary and insignificant role in the spatial and temporal variation in SHF.



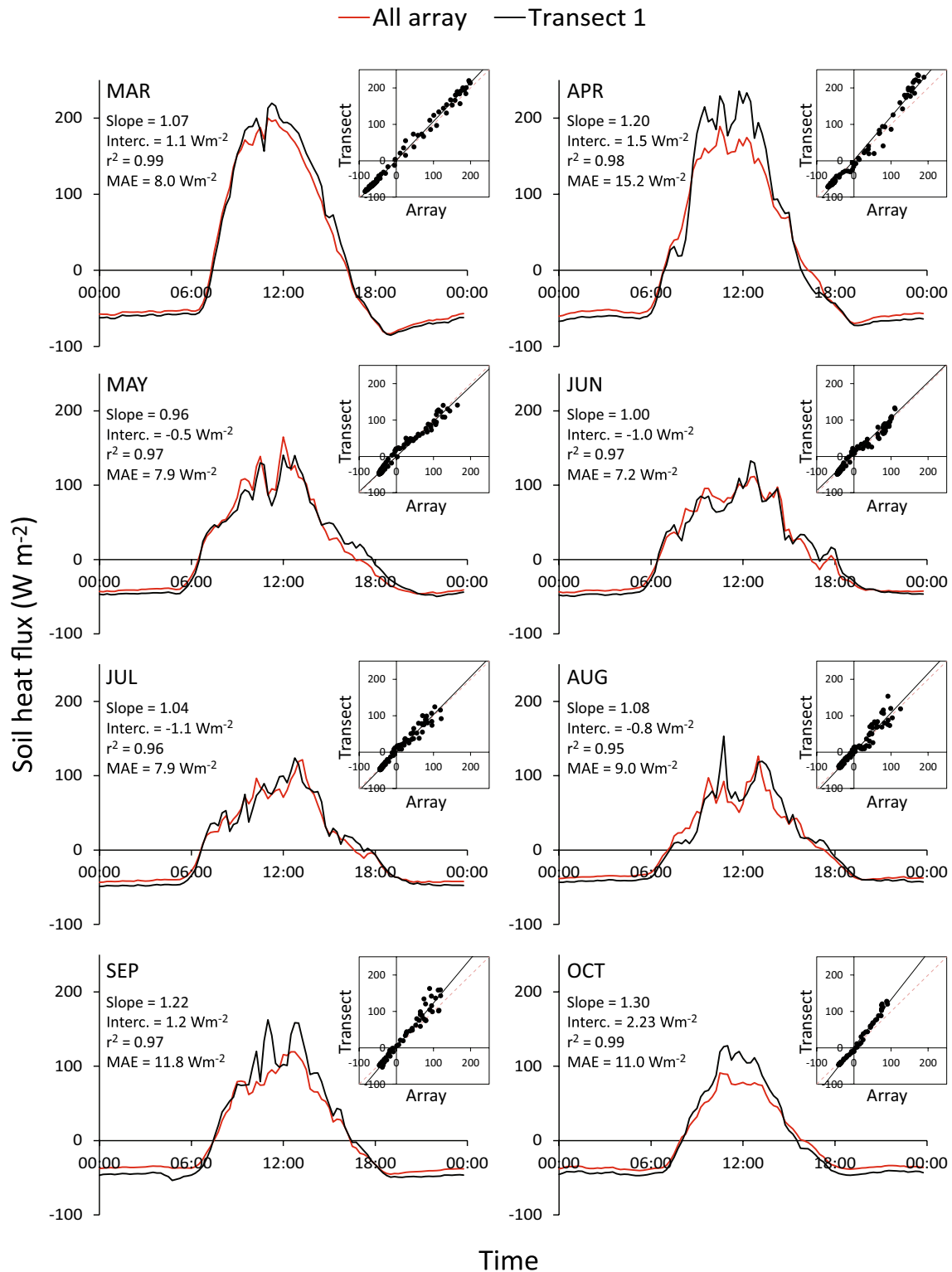


**Fig. 13** The diurnal course of soil heat flux (SHF) derived from averaging the 11 positions in the array and the five positions of the transect for each month from March to October 2016, along with a scatterplot of the transect SHF vs. the array SHF ( $\text{W m}^{-2}$ )

**Fig. 14** Diurnal course of soil heat flux computed as an average of three replicates out of the five replicates of the transect (green shaded lines) compared to the all-five location average (black line) (colour figure online)

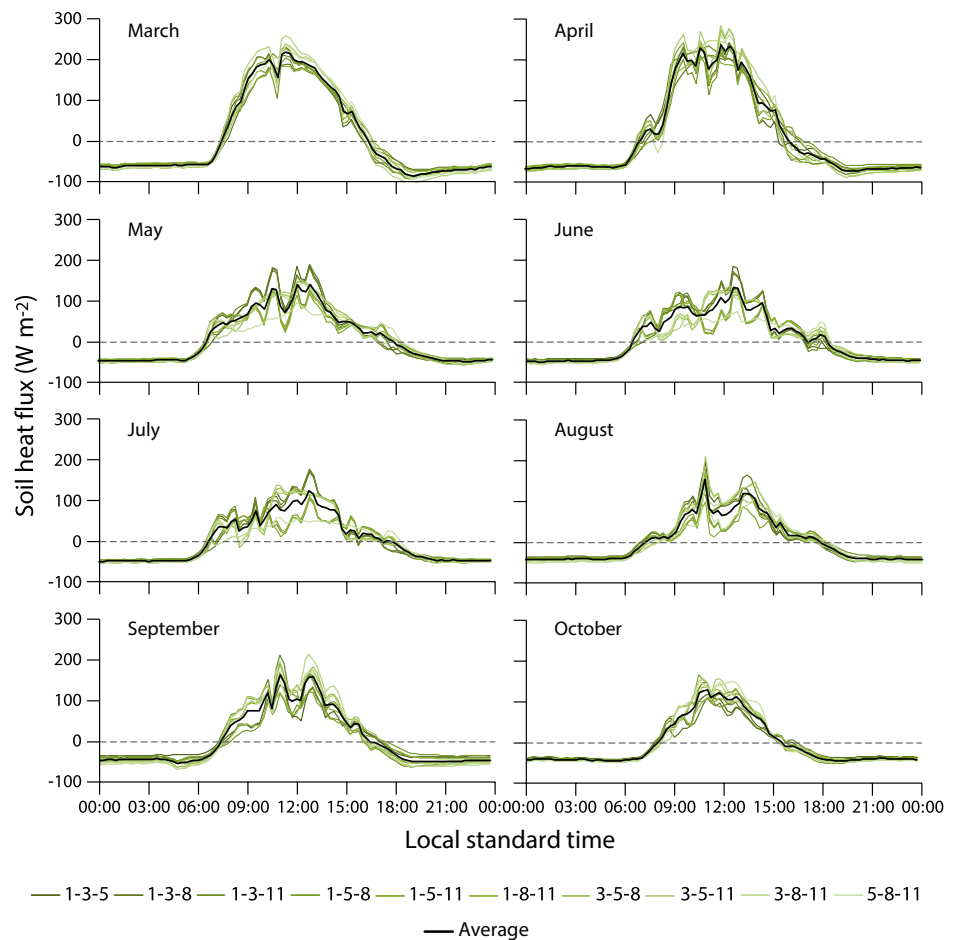


**Table 4** The maximum percent difference calculated by dividing the range of SHF calculated from the ten combinations of three-sensor repetitions versus by the five-sensor transect average

	Mar	Apr	May	Jun	Jul	Aug	Sep	Oct
Nighttime % difference	22	24	24	23	18	32	46	22
Daytime % difference	29	46	78	88	99	94	65	65

The daytime period is 10:00–14:00 PST, and the nighttime is 21:00–03:00 PST. The transition times (from positive to negative SHF and vice versa) were excluded to avoid division by small numbers

Based on the conclusion that SHF variability is primarily dictated by below-canopy incoming solar radiation, it was further hypothesized that for representing the mean SHF of the vine and interrow system, a transect of equally distributed SHF sensors traversing across the vine and interrow should provide an accurate area-average SHF. Indeed, it was found that a transect of five equally distributed sensors across the interrow accurately represented the area-average SHF given by the 11-sensor array, particularly during the growing season.

The reader should note that given the strong effect of radiation reaching the ground on SHF, which is largely

determined by the row orientation and canopy structure, we can only confidently stand behind this conclusion for east–west-oriented rows of vines trained in a bilateral cordon (split canopy) architecture. Previous indications for cotton show a greater variability in SHF across the interrow in north–south-oriented rows compared to an east–west orientation (Agam et al. 2012). It is possible that the five-sensor transect would not be appropriate for vineyards with a north–south row orientation. This topic requires a future investigation.

**Acknowledgements** Funding provided by E.&J. Gallo Winery contributed towards the acquisition and processing of the ground truth data collected during GRAPEX IOPs. In addition, we would like to thank the staff of Viticulture, Chemistry and Enology Division of E.&J. Gallo Winery for the assistance in the collection and processing of field data during GRAPEX IOPs. Finally, this project would not have been possible without the cooperation of Mr. Ernie Dosio of Pacific Agri Lands Management, along with the Borden vineyard staff, for logistical support of GRAPEX field and research activities. The GRAPEX project would like to acknowledge financial support for this research from NASA Applied Sciences-Water Resources Program [Announcement number NNH16ZDA001 N-WATER]. Proposal No. 16-WATER16\_2-0005, Request Number: NNH17AE39I. USDA is an equal opportunity provider and employer.

## Compliance with ethical standards

**Conflict of interest** On behalf of all authors, the corresponding author states that there is no conflict of interest.

## References

- Aase JK, Siddoway FH (1980) Stubble height effects on seasonal microclimate, water-balance, and plant development of no-till winter-wheat. *Agric Meteorol* 21(1):1–20
- Agam N, Kustas WP, Evett SR, Colaizzi PD, Cosh MH, McKee LG (2012) Soil heat flux variability influenced by row direction in irrigated cotton. *Adv Water Resour* 50:31–40
- Battany MC, Grismer ME (2000) Rainfall runoff and erosion in Napa Valley vineyards: effects of slope, cover and surface roughness. *Hydrol Process* 14(7):1289–1304
- Brutsaert W (1982) *Evaporation into the atmosphere: theory, history and applications*. D. Reidel, Boston
- Colaizzi PD, Evett SR, Agam N, Schwartz RC, Kustas WP (2016) Soil heat flux calculation for sunlit and shaded surfaces under row crops: 1. Model development and sensitivity analysis. *Agric For Meteorol* 216:115–128
- Enz JW, Brun LJ, Larsen JK (1988) Evaporation and energy balance for bare and stubble covered soil. *Agric For Meteorol* 43:59–70
- Evett SR, Matthias AD, Warrick AW (1994) Energy balance model of spatially variable evaporation from bare soil. *Soil Sci Soc Am J* 58(6):1604–1611
- Fuchs M, Tanner CB (1968) Calibration and field test of soil heat flux plates. *Soil Sci Soc Am Proc* 32:326–328
- Gao F, Masek J, Schwaller M, Hall F (2006) On the blending of the landsat and MODIS surface reflectance: predicting daily landsat surface reflectance. *IEEE Trans Geosci Remote Sens* 44(8):2207–2218
- Gao F, Anderson MC, Kustas WP, Wang Y (2012) Simple method for retrieving leaf area index from Landsat using MODIS leaf area index products as reference. *SPIE*, pp. 16
- Gao F, Anderson MC, Kustas WP, Houborg R (2014) Retrieving leaf area index from landsat using MODIS LAI products and field measurements. *IEEE Geosci Remote Sens Lett* 11(4):773–777
- Hanks RJ, Tanner CB (1972) Calorimetric and flux meter measurements of soil heat flow. *Soil Sci Soc Am Proc* 36:537–538
- Hatch TA, Hickey CC, Wolf TK (2011) Cover crop, rootstock, and root restriction regulate vegetative growth of cabernet sauvignon in a humid environment. *Am J Enol Vitic* 62(3):298–311
- Heilman JL, McInnes KJ, Savage MJ, Gesch RW, Lascano RJ (1994) Soil and canopy energy balances in a west Texas vineyard. *Agric For Meteorol* 71(1–2):99–114
- Hsieh CI, Huang CW, Kiely G (2009) Long-term estimation of soil heat flux by single layer soil temperature. *Int J Biometeorol* 53(1):113–123
- Idso SB, Aase JK, Jackson RD (1975) Net radiation—soil heat flux relations as influenced by soil water content variations. *Bound-Layer Meteorol* 9(1):113–122
- Jackson LE (2000) Fates and losses of nitrogen from a nitrogen-15-labeled cover crop in an intensively managed vegetable system. *Soil Sci Soc Am J* 64(4):1404–1412
- Kustas WP, Daughtry CST (1990) Estimation of the soil heat flux/net radiation ratio from spectral data. *Agric For Meteorol* 49(3):205–223
- Kustas WP, Prueger JH, Hatfield JL, Ramalingam K, Hipps LE (2000) Variability in soil heat flux from a mesquite dune site. *Agric For Meteorol* 103(3):249–264
- Kustas WP, Agam N, Alfieri JG, McKee LG, Prueger JH, Hipps LE, Howard AM, Heitman JL (2018a) Below canopy radiation divergence in a vineyard: implications on interrow surface energy balance. *Irrig Sci* 10:10. <https://doi.org/10.1007/s002>
- Kustas WP, Anderson MC, Alfieri JG, Knipper K, Torres-Rua A, Parry CK, Nieto H, Agam N, White WA, Gao F, McKee L (2018b) The grape remote sensing atmospheric profile and evapotranspiration experiment. *Bull Am Meteorol Soc* 99(9):1791–1812
- Morlat R, Jacquet A (2003) Grapevine root system and soil characteristics in a vineyard maintained long-term with or without interrow sward. *Am J Enol Vitic* 54(1):1–7
- Payero JO, Neale CMU, Wright JL (2005) Estimating soil heat flux for alfalfa and clipped tall fescue grass. *Appl Eng Agric* 21(3):401–409
- Shao C, Chen J, Li L, Xu W, Chen S, Gwen T, Xu J, Zhang W (2008) Spatial variability in soil heat flux at three Inner Mongolia steppe ecosystems. *Agric For Meteorol* 148(10):1433–1443
- Steenwerth K, Belina KM (2008) Cover crops enhance soil organic matter, carbon dynamics and microbiological function in a vineyard agroecosystem. *Appl Soil Ecol* 40(2):359–369
- Sun L, Gao F, Anderson M, Kustas W, Alsina M, Sanchez L, Sams B, McKee L, Dulaney W, White W, Alfieri J (2017) Daily mapping of 30 m LAI and NDVI for grape yield prediction in California vineyards. *Remote Sens* 9(4):317
- Tesic D, Keller M, Hutton RJ (2007) Influence of vineyard floor management practices on grapevine vegetative growth, yield, and fruit composition. *Am J Enol Vitic* 58(1):1–11
- Watson DF, Philip GM (1985) A refinement of inverse distance weighted interpolation. *Geo-Processing* 2(4):315–327
- White AW, Alsina M, Nieto H, McKee L, Gao F, Kustas WP (2019) Indirect measurement of leaf area index in California vineyards: utility for validation of remote sensing-based retrievals. *Irrig Sci* (this issue)

**Publisher's Note** Springer Nature remains neutral with regard to jurisdictional claims in published maps and institutional affiliations.